Int. J. Heat Mass Transfer. Vol. 28, No. 9, pp. 1711–1719, 1985
Printed in Great Britain

0017-9310/85 $3.00 + 0.00

A steady-state analysis for variable area one- and two-phase thermosyphon loops

EDUARDO RAMOS,*† MIHIR SEN*‡ and CÉSAR TREVIÑO‡

* Departamento de Energía Solar, Instituto de Investigaciones en Materiales, UNAM, 04510 México, D.F., México.
‡ Departamento de Fluidos y Térmica, Facultad de Ingeniería, UNAM, 04510 México, D.F., México

(*Received* 22 *December* 1983 *and in final form* 20 *February* 1985)

Abstract—Multiple solutions for closed thermosyphon loops have been previously found for single-phase, constant area, one-dimensional models. In this paper, this result is further extended to variable area loops. The phase-change thermosyphon is also considered, first with a finite two-phase zone and then using a sharp interface approximation. For entirely different reasons, multiple solutions are also found in this case. The physical basis for multiple solutions in the two-phase loop is discussed in detail with the aid of a particular example.

1. INTRODUCTION

CLOSED thermosyphons are devices capable of transporting heat through natural convection processes and have been used in many applications. For example, they have been studied with reference to their use in solar energy systems [1], nuclear reactor engineering [2], geothermal energy [3, 4], cooling of gas turbine and electronic components [5], arctic and cold climate applications [6], ice making [7, 8] and boiler design [9].

The single-phase thermosyphon uses the density differential due to thermal expansion of a working fluid to maintain the flow. Analyses of such systems have appeared widely in recent literature (see refs. [1–4, 6, 10–13], for instance). A particular feature presented by constant area loops that is discussed in refs. [10, 13] is the multiplicity of solutions.

In two-phase devices, the difference in density of a fluid in its liquid and vapor phases provides the necessary driving force for the circulation. Due to heat input the working fluid boils at the evaporation section; the buoyant vapor moves until it changes to liquid again at the condenser section where heat is extracted from the system. The liquid produced proceeds to the boiling section, thus completing the circuit. Since latent heats are normally much larger than sensible heat changes, the two-phase thermosyphon can be expected to transfer more heat than the single-phase thermosyphon for the same working fluid.

Although a wide variety of geometries have been proposed for the particular applications of two-phase thermosyphons, a general distinction can be made between an enclosure-type system which is basically a cavity filled with the working fluid (like a wickless heat pipe [14]) and the tube loop in which the fluid moves inside a long, closed, possibly variable area duct [7, 15].

The two-phase enclosure-type thermosyphon, though used in practice, is difficult to model since it generally involves solution of the three-dimensional, two-phase governing equations. The loop-type thermosyphon is simpler to model if one-dimensional approximations are made.

In this study, we consider variable area one- and two-phase thermosyphon loops. In Section 2 the one-dimensional governing equations for one- and two-phase thermosyphons are stated. The solution for a single-phase thermosyphon is given in Section 3. The two-phase thermosyphon is discussed in Sections 4 and 5, first considering the existence of a two-phase zone and then with a sharp interface approximation under which the two phases are separated and therefore occupy different regions in the loop. Examples of the applications of the theory presented in Sections 4 and 5 are given in Section 6.

2. ONE-DIMENSIONAL GOVERNING EQUATIONS

For both one- and two-phase thermosyphons we shall consider steady-state, one-dimensional models. The closed loop has an arbitrary shape with a prescribed circular cross section of area $A(x)$, which is a function of the longitudinal coordinate x that runs around the loop. All variables are considered constant across any given section of the loop but vary with x.

Mass conservation in the loop indicates that

$$\rho(x)u(x)A(x) = \dot{m} = \text{const.} \tag{1}$$

where $u(x)$ is the longitudinal fluid velocity, $\rho(x)$ the fluid density and $\dot{m}$ the constant mass flux.

The momentum balance equation in the loop can be written as

$$\rho u\frac{\mathrm{d}u}{\mathrm{d}x} = -\frac{\mathrm{d}p}{\mathrm{d}x} - ku - \tilde{g}\rho \tag{2}$$

where $p(x)$ is the pressure and $\tilde{g}(x)$ the local component of the gravitational acceleration in the direction of the negative x coordinate. The term on the LHS of the equation represents an inertia force while those on the RHS are the pressure, frictional and gravity forces,

† Present address: Laboratorio de Energía Solar, IIM—UNAM, Temixco, Morelos, México.

NOMENCLATURE

A cross-sectional area
C specific heat
D difference in diameter at the interfaces
d, d_1, d_2 distances along the loop (Fig. 1)
e specific internal energy
F_b buoyancy force
F_f frictional force
F_i inertia force
F_p pressure force
g acceleration due to gravity
$\tilde{g}$ local component of the acceleration of gravity
H difference in height between the two interfaces
h specific enthalpy
I integral defined in equation (14)
h_{fg} latent heat
k proportionality factor for the frictional force
L total length of the loop
$\dot{m}$ mass flux defined in equation (1)
p pressure
Q magnitude of the heat transferred
q heat input (or output) per unit length
T temperature
u longitudinal velocity
u_M maximum longitudinal velocity
x longitudinal coordinate
z vertical coordinate.

Greek symbols
β volumetric expansion coefficient
Δ change of properties across an interface
δ Dirac delta function
μ coefficient of viscosity
ρ density.

Subscripts
l liquid
0 reference state
v vapor
1 first solution in Table 1
2 second solution in Table 1
* approximate expressions.

respectively, all per unit volume. In equation (2), we have assumed that the frictional force is a linear function of the velocity. If for further simplification we consider a Poiseuille flow relation based on the local sectional area, we have

$$k(x) = \frac{8\pi\mu}{A(x)} \tag{3}$$

where μ is the viscosity of the fluid.

The one-dimensional energy equation takes the form

$$\dot{m}\frac{\mathrm{d}}{\mathrm{d}x}(h+u^2/2) = q - \dot{m}\tilde{g} \tag{4}$$

where $h(x)$ is the fluid specific enthalpy and $q(x)$ the heat inflow per unit length along the loop. Using equations (1) and (2), and the definition of enthalpy $h = e + p/\rho$, where e is the specific internal energy of the fluid, the energy equation can be conveniently written as

$$\dot{m}\frac{\mathrm{d}e}{\mathrm{d}x} = q + \frac{uAp}{\rho}\frac{\mathrm{d}\rho}{\mathrm{d}x} + Aku^2. \tag{5}$$

The first term on the RHS indicates that the fluid internal energy changes due to external heat sources or sinks. The second and third can be identified with the internal energy changes due to pressure work and viscous dissipation respectively.

Furthermore, we shall have need of an equation of state in order to relate the thermodynamic variables ρ, p, e and h. Different approximations which will be used for the one-phase and two-phase problems will be pointed out in their respective sections.

For future reference, it is convenient to define a vertical coordinate z taken positive upwards, with $z = 0$ at $x = 0$. By definition

$$\tilde{g}(x)\,\mathrm{d}x = g\,\mathrm{d}z \tag{6}$$

where g is the magnitude of the acceleration due to gravity. We notice that the geometrical relation

$$\int_0^L \tilde{g}(x)\,\mathrm{d}x = 0 \tag{7}$$

holds for any three-dimensional form of the closed loop. L is the total length of the loop.

One must also observe that the integral of the energy equation, equation (4), over the entire loop gives

$$\int_0^L q(x)\,\mathrm{d}x = 0 \tag{8}$$

which merely indicates that for a *steady-state solution* to be possible, the total heat input in the system must balance the heat output.

3. SINGLE-PHASE THERMOSYPHON

We consider the Boussinesq approximation in which the fluid properties are assumed constant except for the body force term where we will consider a linear variation of the density with temperature

$$\rho = \rho_0[1 - \beta(T - T_0)]. \tag{9}$$

Here β is the coefficient of volumetric expansion of the fluid and ρ_0 the density at a reference temperature T_0, taken to be that at $x = 0$.

The momentum equation (2) reduces to

$$\rho_0 u\frac{du}{dx} = -\frac{dp}{dx} - ku - \tilde{g}\rho_0\{1-\beta(T-T_0)\}. \quad (10)$$

In this section, we will consider that viscous dissipation and compressibility effects, being of the same order [3], are negligible compared to the heat input, so that the energy equation (5) becomes

$$\dot{m}C\frac{dT}{dx} = q,$$

where we have considered $e = CT$, in terms of the specific heat C. From this

$$T = T_0 + \frac{1}{\dot{m}C}\int_0^x q(x')\,dx'. \quad (11)$$

Integrating equation (10) around the loop and using equation (7), we have

$$\int_0^L ku\,dx = \beta\rho_0\int_0^L \tilde{g}T\,dx. \quad (12)$$

It should be noticed that the integral of the inertia force is zero, which is not so for the two-phase thermosyphon as will be discussed in Section 4. Substituting equations (1) and (11) in (12) we have the following expression for the mass flux

$$\dot{m} = \pm\left[\frac{\beta\rho_0^2}{C}\frac{\int_0^L \tilde{g}(x)\left\{\int_0^x q(x')\,dx'\right\}dx}{\int_0^L \frac{k(x)}{A(x)}\,dx}\right]^{1/2}. \quad (13)$$

The pressure in the system can be obtained on using equations (10) and (11)

$$p(x)-p(0) = -\rho_0\int_0^x u\frac{du}{dx'}\,dx' - \int_0^x ku\,dx' + \frac{\rho_0\beta}{\dot{m}C}\int_0^x \tilde{g}(x') \times\left\{\int_0^{x'} q(\eta)\,d\eta\right\}dx' - \rho_0\int_0^x \tilde{g}(x')\,dx'.$$

If the cross-sectional area of the thermosyphon is constant, we take $A(x) = A_0$, which gives on using equation (3)

$$\dot{m} = \pm\left[\frac{\beta\rho_0^2A_0^2}{8\pi C\mu L}\int_0^L \tilde{g}(x)\left\{\int_0^x q(x')\,dx'\right\}dx\right]^{1/2}.$$

For constant area as well as variable area, we have that for

$$I = \int_0^L \tilde{g}(x)\left\{\int_0^x q(x')\,dx'\right\}dx > 0 \quad (14)$$

two steady-state solutions exist. For $I < 0$ no real solutions exist. This behaviour of the single-phase thermosyphon with known heat flux has been known for some time [13]. This result is now extended to the variable area thermosyphon.

We can show that condition (14) indicates heating at a lower and cooling at a higher level. Integrating by parts, we have

$$I = \left[\int_0^x q(x')\,dx'\int_0^x \tilde{g}(x')\,dx'\right]_0^L - \int_0^L\left[q(x)\int_0^x \tilde{g}(x')\,dx'\right]dx.$$

Using equation (6) and noting that the first term on the RHS of this equation vanishes, we have

$$I = -g\int_0^L q(x)\left[\int_0^{z(x)} dz\right]dx = -g\int_0^L q(x)z(x)\,dx. \quad (15)$$

We introduce the notation $q(x) = q^+(x) - q^-(x)$ where q^+ and q^- are defined as

$$q^+ = \begin{cases} q(x) & \text{for } q(x) > 0 \\ 0 & \text{for } q(x) \leqslant 0 \end{cases}$$

and

$$q^- = \begin{cases} 0 & \text{for } q(x) > 0 \\ -q(x) & \text{for } q(x) \leqslant 0. \end{cases}$$

Equation (8) gives

$$\int_0^L q^+(x)\,dx = \int_0^L q^-(x)\,dx. \quad (16)$$

Using this relation, we can get from condition (14) and equation (15) the relation

$$\frac{\int_0^L q^+(x)z(x)\,dx}{\int_0^L q^+(x)\,dx} < \frac{\int_0^L q^-(x)z(x)\,dx}{\int_0^L q^-(x)\,dx}, \quad (17)$$

which indicates that the overall heating in the loop must take place at a lower vertical height than the overall cooling, since the expressions

$$\int_0^L q^{\pm}z\,dx \Big/ \int_0^L q^{\pm}\,dx,$$

can be interpreted as the heights of the heating (+) and cooling (−) 'centroids'.

The case of point heating and cooling is particularly simple and should be mentioned here in detail. Assume that the heat input in the loop has the form

$$q(x) = Q[\delta(x-x_1)-\delta(x-x_2)]$$

where δ represents the Dirac delta function and the constant Q the magnitude of the heat input or output. In this case, from (14)

$$I = Q\int_0^L \tilde{g}(x)\left\{\int_0^x [\delta(x'-x_1)-\delta(x'-x_2)]\,dx'\right\}dx = Q\int_{x_1}^{x_2} \tilde{g}(x)\,dx = Qg[z(x_2)-z(x_1)]. \quad (18)$$

The condition $I > 0$ thus indicates that the heating point ($x = x_1$) should be at a lower position than the cooling point ($x = x_2$) for the steady-state solution to exist.

4. PHASE CHANGE THERMOSYPHON WITH TWO-PHASE ZONE

The loop geometry considered in this case is similar to that of Section 3 and is shown in Fig. 1. We assume heat outflow $q_1(x)$ per unit length in the region $0 < x \leqslant d_1$ where the working fluid coexists in liquid and vapor form. Fluid in the region $d_1 < x \leqslant d_2$ is in the liquid state. In $d_2 < x \leqslant d$ we have heat inflow $q_2(x)$ per unit length so that both liquid and vapor phases are again present in this region. Fluid in the region $d < x \leqslant L$ exists only in the vapor state. The parts of the loop not corresponding to two-phase zones are considered adiabatic.

Integrating equation (2) around the loop, we have

$$\int_0^L \rho u \frac{\mathrm{d}u}{\mathrm{d}x}\,\mathrm{d}x = -\int_0^L \tilde{g}\rho\,\mathrm{d}x - \int_0^L ku\,\mathrm{d}x, \qquad (19)$$

which on using equation (1) reduces to

$$\dot{m}^2 \int_0^L \frac{1}{A}\frac{\mathrm{d}}{\mathrm{d}x}(1/\rho A)\,\mathrm{d}x + \dot{m}\int_0^L \frac{k}{\rho A}\,\mathrm{d}x + \int_0^L \tilde{g}\rho\,\mathrm{d}x = 0. \qquad (20)$$

This equation for the mass flux $\dot{m}$ is coupled to the energy and state equations through the density $\rho(x)$ and viscosity $\mu(x)$. Some physical insight can be gained, however, on considering some decoupling approximations.

For a start, the density and viscosity in the liquid and vapor regions can be considered constant (denoted by the subscripts 'l' and'v' respectively). In the two-phase zones, these properties are taken to be known functions of x, varying linearly from one phase to the other. Choosing these linear interpolation functions, the integrals in equation (20) can be evaluated in terms of the liquid and vapor properties as well as the known area function $A(x)$. A quadratic equation in the mass flux remains. The roots can be both complex, in which case no steady-state solution to the assumed liquid–vapor configuration exists. More interesting is the case in which two real solutions can be obtained. These can be of the same sign, i.e. in the same direction, or of different signs and hence in different directions. As a special case two identical solutions can also be obtained. A very different situation results when the cross-sectional area of the thermosyphon is constant. The inertia force term disappears and the balance is only between the frictional forces and the gravity forces. There is a unique solution. This special case has been dealt with in detail in [16] using a sharp interface approximation (see Section 5).

It should be emphasized that the multiple nature of the steady two-phase thermosyphon is *not* due to the rather simplistic assumption we have made regarding the frictional forces. Other more realistic empirical relations can be used. However, the point is that in the presence of the quadratic inertia term, at least two solutions can be obtained in general.

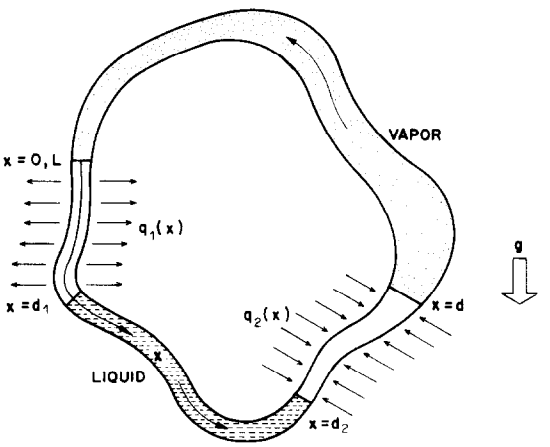

FIG. 1. The two-phase thermosyphon.

5. SHARP INTERFACE APPROXIMATION

Useful information can be obtained if we consider the limit when $d_1 \to 0$ and $d_2 \to d$. The liquid and vapor phases are entirely separated. When the two-phase zones vanish, contributions to the integrals in equation (20) from these regions are zero. Equation (20) becomes

$$a\dot{m}^2 + b\dot{m} + c = 0 \qquad (21)$$

where

$$a = \tfrac{1}{2}(1/\rho_v - 1/\rho_l)\{1/A^2(d) - 1/A^2(0)\},$$

$$b = 1/\rho_l \int_0^d \frac{k_l}{A}\,\mathrm{d}x + 1/\rho_v \int_d^L \frac{k_v}{A}\,\mathrm{d}x,$$

$$c = \rho_l \int_0^d \tilde{g}\,\mathrm{d}x + \rho_v \int_d^L \tilde{g}\,\mathrm{d}x.$$

The last coefficient, by virtue of equations (7) and then (6), can be written as

$$c = (\rho_l - \rho_v)\int_0^d \tilde{g}\,\mathrm{d}x = (\rho_l - \rho_v)(z_d - z_0)g$$

where z_0 and z_d correspond to the vertical height of the two interfaces. Since $\rho_l > \rho_v$, c will be negative if the vapor to liquid interface is higher than the liquid to vapor interface. The coefficient b is always positive while a will be positive for $A(0) > A(d)$ and negative for $A(0) < A(d)$.

No real solution of (21) will be obtained for

$$b^2 - 4ac < 0,$$

otherwise two real solutions will exist. In special cases, if a and c are of different signs, two solutions of different signs exist. This will occur for $z_0 > z_d$, $A(0) > A(d)$ and for $z_0 < z_d$, $A(0) < A(d)$, i.e. if the cross-sectional area at

the higher interface is larger than that at the other interface. In the particular case of a constant cross-sectional area loop, $A(0) = A(d) = A_0$ and hence (21) becomes linear so that the only solution is

$$\dot{m} = \frac{A_0^2(\rho_l - \rho_v)(z_0 - z_d)g}{\dfrac{k_l d}{\rho_l} + \dfrac{k_v(L-d)}{\rho_v}}, \tag{22}$$

which is the mass flux obtained in [16]. In this constant area case, the fluid will flow in the direction of gravity in the branch that contains liquid at a higher level.

Under the sharp interface approximation, the heat flux in the energy equation (4) can be represented by

$$q(x) = Q\{\delta(x-d) - \delta(x)\}.$$

Longitudinal derivatives which appear in equations (2) and (4) cease to make sense at the sharp interfaces. However, we can integrate the expressions before taking the limit. The integrals are finite and yield jump conditions at the interfaces.

Integrating (4) from $x = 0^-$ to $x = 0^+$, we have

$$\dot{m}\Delta_0(h + u^2/2) = Q, \tag{23}$$

where Δ_0 represents a change across the interface at $x = 0$. Since both the enthalpy and the velocity in the liquid are small compared to their corresponding values for the vapor, $\Delta_0(h+u^2/2) < 0$ so that Q and $\dot{m}$ have different signs. For an anticlockwise motion in Fig. 1, heat will have to be extracted from the fluid at $x = 0$ and consequently added at $x = d$.

In order to find the heat transported by the loop, we will assume that the system is under saturation conditions, i.e. all the heat that is being given to the system is used just to evaporate the liquid, and all the heat withdrawn from the system is condensation heat. None of the external energy exchange goes to modify the temperature of the system. In most practical cases, kinetic energy changes are very small compared to enthalpy changes. The enthalpy change across the interfaces can be taken to be the latent heat even though the pressure is slightly different on either side of the interfaces. Under this approximation

$$\dot{m}h_{fg} = 0 \tag{24}$$

where h_{fg} is the latent heat of evaporation per unit mass.

Of course, higher heat fluxes can be transferred if the liquid is permitted to be subcooled and/or the vapor superheated. In this sense, heat flux Q is the minimum needed to obtain two-phase circulation.

Once the mass flow rate is known, the liquid and vapor velocities are obtained using equation (1). The pressure in the system as a function of the x coordinate is obtained from equation (2)

$$-p(x) + p(0) - \int_0^x \rho u \frac{du}{dx'}\,dx' - \int_0^x ku\,dx' - \int_0^x \tilde{g}\rho\,dx' = 0 \tag{25}$$

where the pressure $p(0)$ at $x = 0$ has to be prescribed.

Equation (25) can be rewritten by using (1)

$$-p(x) + p(0) - \dot{m}^2 \int_0^x \frac{1}{A}\frac{d}{dx'}(1/\rho A)\,dx' - \dot{m}\int_0^x \frac{k}{\rho A}\,dx' - \int_0^x \tilde{g}\rho\,dx' = 0. \tag{26}$$

While performing the integrals in equation (26) care must be taken when the liquid–vapor interfaces lie within the integration interval. At the interfaces, the following conditions must be satisfied.

$$\Delta_0(p) = -\frac{\dot{m}^2}{A^2}\Delta_0\left(\frac{1}{\rho}\right), \quad \Delta_d(p) = -\frac{\dot{m}^2}{A^2}\Delta_d\left(\frac{1}{\rho}\right) \tag{27}$$

where Δ_0 and Δ_d denote the change in the argument across the $x = 0$ and $x = d$ interfaces, respectively. In obtaining equation (27) we have made use of the sharp interface approximation. Considering the two-phase zone to be negligibly narrow, the cross-section of the conduit can be assumed constant. Also, interaction with the walls and gravitational effects can be neglected.

6. PARTICULAR EXAMPLES

In this section, particular examples of two-phase thermosyphons are discussed in detail. Since the objective is to help in the physical understanding of the problem, all values are kept in their dimensional forms. The thermosyphon geometry shown in Fig. 2 has been arbitrarily chosen, but it is expected that a system of such a design can be easily built in the laboratory for experimental studies.

The thermosyphon cross-section is circular and its centerline along which the coordinate x runs, describes a rectangle. The total length of the loop is 1 m. The diameters of the wide and narrow sections are 0.1 and 0.02 m, respectively. The wider tube is connected to the narrower one by 'conical' tubes where the cross-sectional area varies linearly. The length of the upper and lower 'conical' sections are 0.05 and 0.07 m, respectively.

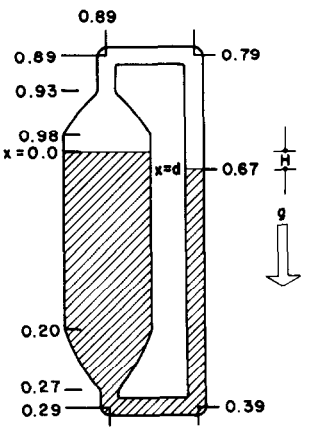

FIG. 2. Geometry of the loop of the particular examples discussed in Section 6. Distances in m from one interface and along the centerline are indicated.

Table 1. Physical properties of working fluids and numerical values for the two possible solutions.

	Water	Freon 11	Nitrogen	
ρ_l (kg m^{-3})	988	1533	818	
ρ_v (kg m^{-3})	0.60	2.59	3.81	
μ_l (kg s^{-1} m^{-1})	2.83×10^{-4}	5.50×10^{-4}	1.9×10^{-4}	Physical
μ_v (kg s^{-1} m^{-1})	1.21×10^{-5}	1.01×10^{-5}	0.51×10^{-5}	properties
h_{fg} (J kg^{-1})	2.26×10^{6}	0.190×10^{6}	0.205×10^{6}	
$\dot{m}$ (kg s^{-1})	3.32×10^{-3}	8.69×10^{-3}	7.73×10^{-3}	
u_M (ms^{-1})	17.64	10.68	6.46	
$a\dot{m}^2$ (Pa)	93.09	147.34	78.9	First
$b\dot{m}$ (Pa)	4.67	2.63	0.890	solution
c (Pa)	−97.76	−149.98	−79.79	
Q (W)	7506	1652	1447	
$\dot{m}$ (kg s^{-1})	-3.49×10^{-3}	−8.85	−7.81	
u_M (m s^{-1})	−18.52	−10.88	−7.15	
$a\dot{m}^2$ (Pa)	102.67	152.66	80.69	Second
$b\dot{m}$ (Pa)	−4.91	−2.68	−0.90	solution
c (Pa)	−97.76	149.98	−79.79	
Q (W)	−7983	−1681	−1464	

Values of the physical properties are from Dunn and Reay [17], at $T = 373$ K and $p = 101$ kPa for water, $T = 273$ K and $p = 43$ kPa for Freon 11 and $T = 73$ K and $p = 74$ kPa for nitrogen.

We assume that the heat input (and output) is such that the liquid level in the wider section is maintained 0.01 m above that in the narrower section. According to the discussion in Section 5, this allows steady-state conditions. No steady-state flow would be possible if the interface in the narrow section were higher than that in the other. Equation (21) can be used to calculate the mass flow rate. Using water, Freon 11 and nitrogen as working fluids, the results shown in Table 1 are found. As discussed in Section 5, motion is possible in both clockwise and anticlockwise directions. For clockwise motion, heat must be given to the system at $x = 0$ and withdrawn at $x = d$. The opposite will be true for anticlockwise motion in which heat is added to the fluid at a lower level and transferred out at a higher. The maximum velocity u_M is the velocity calculated in the vapor phase, at the narrower section. Table 1 also contains the three different terms in equation (21), $a\dot{m}^2$, $b\dot{m}$ and c which represent the inertia, frictional and buoyancy force per unit area, respectively. Their numerical values indicate that in this example frictional effects are negligible compared to inertia and buoyancy effects, suggesting the approximation $\dot{m}b \simeq 0$. This yields the following expressions for the mass flow rate and the maximum velocity:

$$\dot{m}^* \simeq \pm\left\{\frac{2\rho_v\rho_l gH}{1/A^2(d) - 1/A^2(0)}\right\}^{1/2}$$

and

$$u_M^* \simeq \pm\left\{\frac{2\rho_l/\rho_v gH}{1 - A^2(d)/A^2(0)}\right\}^{1/2} \qquad (28)$$

where H is the difference in height between the two interfaces.

The individual terms in the momentum balance equation (26) as functions of the coordinate x are obtained once the mass flow rate has been determined. These profiles for $\dot{m}$ from the first solution in Table 1 are shown in Fig. 3 for water as the working fluid, and $p(0) = 0$. Interpretation of the profile is aided by a diagram of the unfolded loop and the gravity acceleration function given in the lower part of the figure as functions of x. For each location in the loop, the sum of the pressure force (F_p), frictional force (F_f), buoyancy force (F_b), and inertia force (F_i) adds to zero. In the liquid region and in the narrow vapor region, the most important effects are by far those due to pressure and buoyancy.

In the wider vapor region, the inertia forces also play an important role. This is shown in the inset of Fig. 3. Also shown in this inset are the profiles obtained from the second solution in Table 1 which are indistinguishable from those drawn using $\dot{m}$ from the first solution in the rest of the loop.

In order to analyze the effect of the difference in the height of the two liquid–vapor interfaces H, Fig. 4 shows the mass flow rate ($\dot{m}$), the maximum velocity (u_M), the heat input (Q) and approximate values of $\dot{m}^*$ and u_M^* (shown as + and × respectively) from equation (28) as functions of H. Subscripts 1 and 2 are used to denote the two different solutions. Obviously, the theory presented here is only valid for values of u_M small compared to the speed of sound in vapor (for saturated water vapor this is about 443 m s^{-1} at 100°C).

The effect of the difference in diameters at the two interfaces (D) is shown in Fig. 5 where $\dot{m}_1$ and $\dot{m}_2$ are presented as functions of D. Whenever this difference $D > 0.01$ m, the two mass flow rates have approximately the same magnitude but are different in sign.

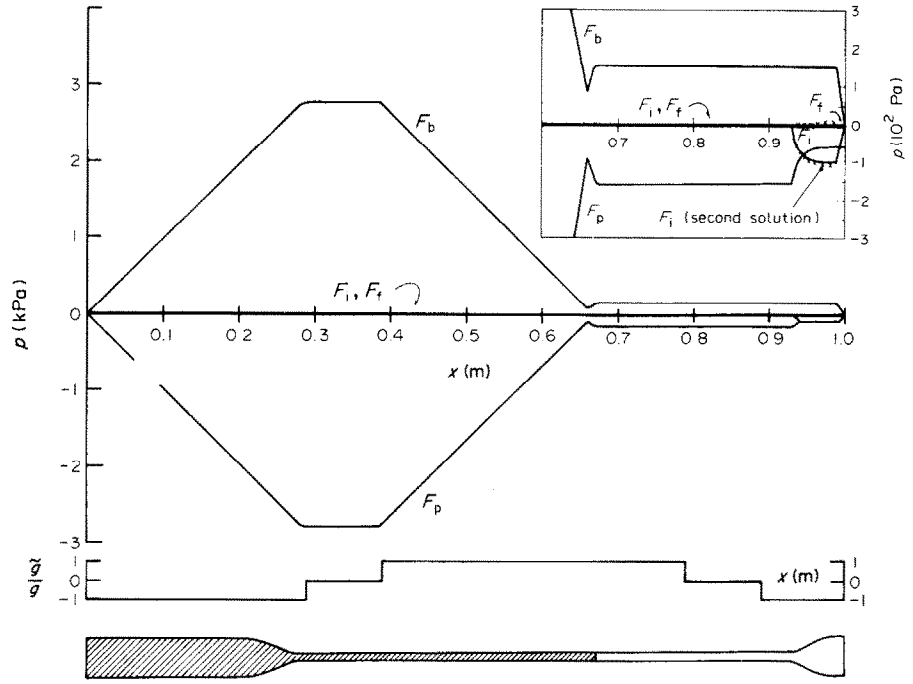

FIG. 3. Forces interacting in the flow as functions of the longitudinal coordinate x for the first solution in Table 1. The profiles for the second solution are denoted by $\times$.

When $D \to 0$, the negative mass flow becomes unbounded while the positive solution tends to the constant area value, given in equation (22). Obviously, when the velocity for $\dot{m}_2$ grows beyond a certain limit other effects not considered in this model would appear to prevent it from growing infinitely large. Apart from this restriction, the two solutions $\dot{m}_1$ and $\dot{m}_2$ are equally possible. We merely demonstrate the existence of these

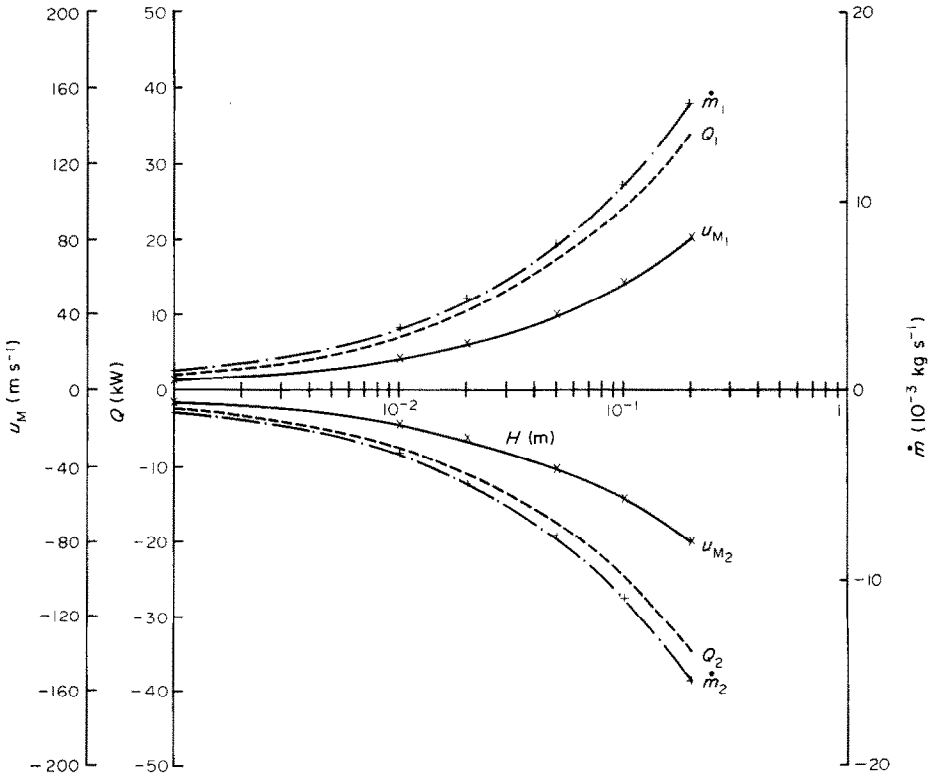

FIG. 4. Flow characteristics as functions of interface height difference (H).

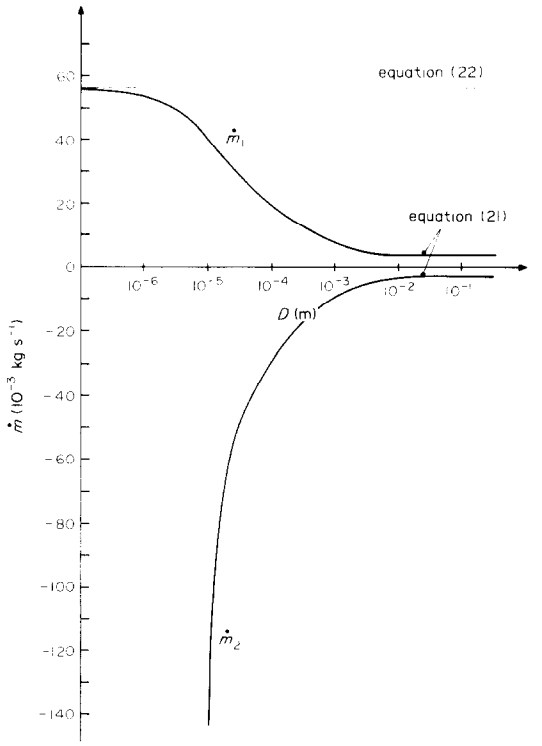

FIG. 5. Mass flow rates as functions of the diameter difference at the interfaces (D).

two solutions, although we cannot yet advance any opinion with respect to their stability.

7. DISCUSSION AND CONCLUSION

The flow in one- and two-phase variable area loops has been analyzed for steady-state conditions. It was demonstrated that in both cases, multiple solutions for the flow are possible, although the physical conditions that permit such situations are different in each case. In the single-phase thermosyphon interplay between the buoyancy and viscosity effects leads to the two solutions. In the two-phase case, non-linearity of the inertia forces permits the existence of two possible solutions.

For a single-phase thermosyphon, it was shown that heat can only be transferred under steady-state conditions from a lower point to a higher one. This is not so for a two-phase thermosyphon where heat can be transferred from one point to the other regardless of their relative position, provided some geometrical conditions are fulfilled. Although multiple solutions have been found in this study, it is important to remark that one or both solutions can be unstable. This point constitutes a topic of further research.

For the two-phase thermosyphon, a particular example illustrates the different effects that take place in the system. Frictional forces are found to be unimportant, permitting simplified expressions to be used for calculating the mass flow rate. Although this is only an example, it is expected that the features discussed in this context apply also to other systems.

Acknowledgement—Partial support was received for this project from CONACYT and Fondo de Estudios e Investigaciones Ricardo J. Zevada under separate grants.

REFERENCES

1. A. Mertol, W. Place, T. Webster and R. Greif, Detailed loop model (DLM) analysis of liquid solar thermosiphons with heat exchangers, *J. Sol. Energy* **27**, 367–386 (1981).
2. A. K. Agrawal, I. K. Madni, J. G. Guppy and W. L. Weaver, Dynamic simulation of LMFBR plant under natural circulation, *J. Heat Transfer* **103**, 312–318 (1981).
3. H. H. Bau and K. E. Torrance, On the effects of viscous dissipation and pressure work in free convection loops, *Int. J. Heat Mass Transfer* **26**, 727–734 (1983).
4. D. B. Kreitlow, G. M. Reistad, C. R. Miles and G. G. Culver, Thermosyphon models for downhole heat exchanger applications in shallow geothermal systems, *J. Heat Transfer* **100**, 713–719 (1978).
5. D. Japikse, Advances in thermosyphon technology. In *Advances in Heat Transfer* (edited by T. F. Irvine and J. P. Hartnett), Vol. 9, pp. 1–111. Academic Press, New York (1973).
6. R. L. Reid, J. S. Tennant and K. W. Childs, The modeling of a thermosyphon type permafrost protection device, *J. Heat Transfer* **97**, 382–386 (1975).
7. S. L. Chao and R. J. Schoenhals, An experimental study of a closed two-phase thermosyphon for ice production. 20th. Joint ASME/AIChE National Heat Transfer Conference Milwaukee, Wisconsin (1981) paper No. 81-HT-16.
8. R. L. McClain and K. T. Yang, An analytical study of a two-phase thermosyphon for ice production in a long term cold storage. *ASME/JSME Thermal Engng Joint Conf. Proc.*, Vol. 2, pp. 387–394. American Society of Mechanical Engineers (1983).
9. D. B. Bandy and S. G. Bankoff, Optimal design of a natural-circulation boiling-water channel. In *Progress in Heat and Mass Transfer* (edited by U. Grigull and E. Hahne), Vol. 1, pp. 425–471. Pergamon Press, Oxford (1969).
10. M. Sen and C. Treviño, One-dimensional thermosyphon analysis, *Latin Am. J. Heat Mass Transfer* **7**, 135–150 (1983).
11. M. Sen and C. Treviño, Dynamic analysis of one-dimensional thermosyphon model, *J. therm. Engng.* **3**, 15–20 (1982).
12. L. A. Rubenfeld and W. L. Siegmann, Nonlinear dynamic theory for a double-diffusive convection model, *SIAM J. appl. Math.* **32**, 871–894 (1977).
13. P. S. Damerell and R. J. Schoenhals, Flow in a toroidal thermosyphon with angular displacement of heated and cooled sections, *J. Heat Transfer* **101**, 672–676 (1979).
14. F. E. Andros and L. W. Florshuetz, Heat transfer characteristics of the two-phase closed thermosyphon (wickless heat pipe). *Proc. Seventh Int. Heat Transfer Conference*, Munich, Vol. 4, pp. 187–192 (1982).
15. A. F. M. Ali and T. W. McDonald, Thermosyphon loop performance characteristics: part 2. Simulation program. *Trans. Am. Soc. Heat. Refrig. Air-Condit. Engrs.* **83**, 260–278 (1979).
16. M. Sen, C. Treviño, E. Ramos and B. C. Raychaudhuri, Natural circulation driven two phase flow loops. In *Alternative Energy Sources* V. Part A: *Solar Radiation/Collection/Storage* (edited by T. N. Veziroglu), pp. 435–441. Elsevier, Amsterdam (1983).
17. P. D. Dunn and D. A. Reay, *Heat Pipes*, pp. 294, 295 and 299. Pergamon Press, Oxford (1978).

ANALYSE EN REGIME PERMANENT DE BOUCLES DE THERMOSIPHON A SECTION VARIABLE ET A UNE OU DEUX PHASES

Résumé—Des solutions multiples pour des boucles fermées de thermosiphon ont été précédemment trouvées pour des modèles monodimensionnels à section constante. Ce résultat est ici étendu à des boucles de section variable. On considère aussi le thermosiphon avec changement de phase, tout d'abord avec une zone finie diphasique puis en utilisant une approximation d'interface. Pour des raisons totalement différentes, on trouve aussi, dans ces cas, des solutions multiples. La raison physique de ces solutions multiples dans la boucle à deux phases est discutée en détail à l'aide d'un exemple particulier.

UNTERSUCHUNG VON EIN- UND ZWEIPHASEN-THERMOSYPHON-SCHLEIFEN VARIABLER FLÄCHE IM STATIONÄREN ZUSTAND

Zusammenfassung—Für einphasige eindimensionale Modelle einer geschlossenen Thermosyphon-Schleife von konstanter Fläche sind bereits früher Mehrfach-Lösungen gefunden worden. In dieser Arbeit werden diese Ergebnisse auf Schleifenanordnungen mit veränderlicher Fläche ausgeweitet. Ebenso wird ein Thermosyphon mit Phasenänderungen betrachtet, und zwar zuerst mit einem begrenzten Zweiphasen-Gebiet und dann unter Verwendung einer scharfen Grenzfläche. Aus völlig anderen Gründen ergeben sich auch in diesem Fall Mehrfach-Lösungen. Die physikalische Grundlage für diese Mehrfach-Lösungen bei der Zweiphasen-Schleifen-Anordnung wird unter Zuhilfenahme eines Beispiels im einzelnen erörtert.

АНАЛИЗ СТАЦИОНАРНОГО СОСТОЯНИЯ ПЕРЕМЕННОЙ ПЛОЩАДИ ОДНО- И ДВУХФАЗНЫХ КОЛЬЦЕВЫХ ТЕРМОСИФОНОВ

Аннотация—Ранее были найдены семейства решений для закрытых кольцевых термосифонов для однородных одномерных моделей с постоянной площадью. В данной работе полученный результат распространяется на случай контуров переменной площади. Рассматривается также двухфазный термосифон вначале с ограниченной двухфазной зоной, а затем с применением аппроксимации явно выраженной поверхности раздела фаз. В этом случае также найдены множества решений для различных условий. Физические принципы получения множества решений в двухфазных контурах детально рассматриваются на основе частного примера.